The Landes experiment - biosphere-atmosphere exchanges of ozone and aerosol-particles above a pine forest

Eric Lamaud, Yves Brunet, Alain Labatut, Alain Lopez, Jacques Fontan, Aimé Druilhet

JOURNAL OF GEOPHYSICAL RESEARCH, VOL. 99, NO. D8, PAGES 16,511–16,521, AUGUST 20, 1994

The Landes experiment: Biosphere-atmosphere exchanges of ozone and aerosol particles above a pine forest

E. Lamaud,[1] Y. Brunet,[2] A. Labatut,[1] A. Lopez,[1] J. Fontan,[1] and A. Druilhet[1]

Abstract. An experiment was conducted in a pine forest in southwestern France during late spring 1992. The aim was fourfold: testing various flux measurement methodologies for chemically reactive species; quantifying the exchanges between the forest and the atmosphere; analyzing the involved mechanisms; and studying their influence on the chemistry of the surface boundary layer. This paper presents preliminary results obtained on the dry deposition of ozone and submicronic aerosol particles, measured using eddy correlation. Once properly normalized, the spectra and cospectra of all scalar species exhibit universal shapes over the whole frequency range. However, evidence is provided that under some meteorological conditions the time series of turbulent variables can be affected by nonstationary trends, or low-frequency fluctuations that do not contribute to vertical transfer but whose presence can induce large errors in the calculated fluxes. The time variations of the deposition velocities for ozone and aerosol particles are then presented over 2 days with different meteorological conditions. The deposition velocities are shown to be consistent with other reported studies. Dry deposition of ozone appears to be mainly governed by the stomatal resistance, whereas friction velocity and atmospheric instability in the boundary layer seem to govern the deposition of aerosol particles.

1. Introduction

Soil and vegetation can be a source or a sink for atmospheric constituents. They always act as a sink for ozone. This is most often the case for aerosol particles too, but the soil may also be a source of particles in the case of wind erosion. The decomposition of soil organic matter releases carbon dioxide into the atmosphere, but the vegetation acts both as a sink (photosynthesis) and a source (respiration). Plants emit terpenes; nitrogen compounds are involved in complex chemical cycles and can be emitted or uptaken by the soil and the vegetation.

The strength of the various sinks and sources depends on several factors, including (1) the aerodynamic resistance to turbulent transfer between the vegetation or the soil and the atmosphere; (2) the leaf boundary layer resistance; (3) the stomatal resistance, expressing the stomatal control of gas diffusion into or outside of the leaves; and (4) various other resistances, including cuticular, mesophyll, and soil resistances [*Hosker and Lindberg*, 1982; *Song-Miao et al.*, 1990; *Wesely*, 1989]. In the case of particles, other effects may also be acting, such as inertial interception, impaction, bounce-off, gravitational sedimentation [*Slinn*, 1982; *Sievering*, 1987; *Wesely et al.*, 1985]. The size distribution also influences the removal rate of particles.

[1]Laboratoire d'Aérologie, Université Paul Sabatier, Toulouse, France.

[2]Laboratoire de Bioclimatologie, Institut National de la Recherche Agronomique, Villenave d'Ornon, France.

Paper number 94JD00668.
0148-0227/94/94JD-00668$05.00

The aerodynamic resistance is supposed to be identical for all scalars, and large fractions of the vertical fluxes are transported by the same turbulent eddies, which also ensure the transport of momentum, water vapor, and sensible heat. However, the other mechanisms of deposition or emission may be different for the various atmospheric constituents. In other words, their deposition velocities must share common properties but also exhibit differences. It is therefore informative to compare the exchanges and the source-sink strengths for entities such as ozone, aerosol particles, CO_2, nitrogen compounds, and terpenes. This can provide good insight into the various mechanisms involved, which is a necessity for studying the transfer of trace gases in the lower atmosphere, a topic of high importance.

For this purpose, measurements were performed in the forested area of "Les Landes", located in southwestern France. This forest is one of the largest in western Europe. It is located along the Atlantic coast over an area of 1 million ha. About 90% of the area is covered by trees, and the remaining 10% includes cultivated and fertilized land where corn is the main crop. The forested part consists of 85% resinous trees (maritime pine) and 15% deciduous trees. The region is not densely populated and the local sources of pollution, coming from combustion of fossil fuel, are not intense. When the air masses are westerly, the forest is exposed to little pollution. In anticyclonic situations the pollutants come from the continent. The town of Bordeaux is located northeast of the forest and in some particular meteorological situations the forest can be influenced by the city plume. So, the level of concentration of pollutants can vary substantially, depending on the synoptic situation. The whole region is very flat, with rather simple flow patterns [*Fontan et al.*, 1992]. The Landes forest, as a result of its vegetal composition, is a useful site for studying the influ-

ence of biogenic hydrocarbon emission on the chemistry of the atmospheric boundary layer [*Lopez et al.*, 1988].

This first experiment was performed in June 1992, with four major objectives: testing various flux measurement methodologies for chemically reactive species; quantifying the exchanges between the forest and the atmosphere; analyzing the involved mechanisms; and studying the influence of these exchanges on the chemistry of the surface boundary layer. The biogenic emissions of terpenes (α- and β-pinene) are presented in a companion paper [*Simon et al.*, this issue]. Results on some aspects of the nitrogen cycle in the forest are presented in another companion paper [*Jambert et al.*, this issue]. The results on CO_2 measurements will be presented in a later paper.

Here, we focus on the vertical fluxes of O_3 and aerosol particles. A substantial part of this study is devoted to problems encountered when performing eddy correlation measurements of these fluxes and related to the occasional presence of large, low-frequency fluctuations of concentration, linked with advective motions. A few quantitative results on daily variations of dry deposition velocities are then presented. As the present paper is meant to be a "reference" paper for the 1992 Landes experiment, we also provide a detailed description of the site, the instrumentation, and the meteorological conditions encountered, even if only part of this information is actually used here.

2. Experimental Site and Instrumentation

The experimental site is located in the center of a flat, homogeneous field covering about 10 km^2 in the region of Pierroton, a city located 25 km southwest of Bordeaux. The vegetation canopy consists of maritime pine (*Pinus pinaster* Ait.) with a short (less than 1 m) gramineous understory on a sandy soil. The canopy height is 15 m and the leaf area index of the trees is about 3. The site has a good fetch, longer than 1 km for the prevailing wind directions.

The site is permanently equipped with a 25-m-high tower, on which a number of instruments were installed. A sketch of the experimental setup is displayed in Figure 1. The following measurements were performed:

1. Wind direction, global radiation, net radiation.

2. Mean profiles of microclimatic parameters (mean horizontal velocity U, air temperature T_a, and wet-bulb temperature T_w) at heights 0.5, 2.5, 5.0, 7.6, 10.1, 13.7, 16.2, 18.2, 20.75, 22.8, and 25.0 m.

3. Mean concentration profiles of CO_2, ozone, aerosols, nitrogen oxides and terpenic hydrocarbons. The experimental devices used are as follows: CO_2, infrared analyzer (ADC, model MK3); ozone, UV absorption analyzer (S.A. Environnement, model 1003 AH); aerosols, condensation nuclei counter (TSI, model 3022); nitrogen oxydes (NO, NO_2), chemiluminescence analyzer (Luminox LMA3); terpenic hydrocarbons, preconcentration on Tenax GC, thermodesorption, and analysis by gas phase chromatography, using a technique developed by *Clément et al.* [1993].

4. Vertical turbulent fluxes of momentum, sensible heat, water vapor, CO_2, ozone, and aerosols, using eddy correlation. All fluxes were measured at the top of the tower (25 m). Additional flux measurements were performed below the forest crown (at 6 m) and at various heights within the crown, for momentum, sensible heat, water vapor, and CO_2. Data acquisition was made at frequencies of 10 and 20 Hz on two separate microcomputers. For perfect synchronization, several channels were simultaneously recorded on both systems. All raw data were saved on magnetic tapes for later processing. The experimental devices include four three-dimensional sonic anemometers (Dobbie Instruments, model PAC-100; Applied Technologies, model SWS-211/3EK; Gill Instruments, model Solent) and several fast-response analyzers: three infrared sensors for CO_2 and H_2O (Advanet Systems, model E009), one ozone analyzer, and one aerosol analyzer. The ozone analyzer is a chemilumines-

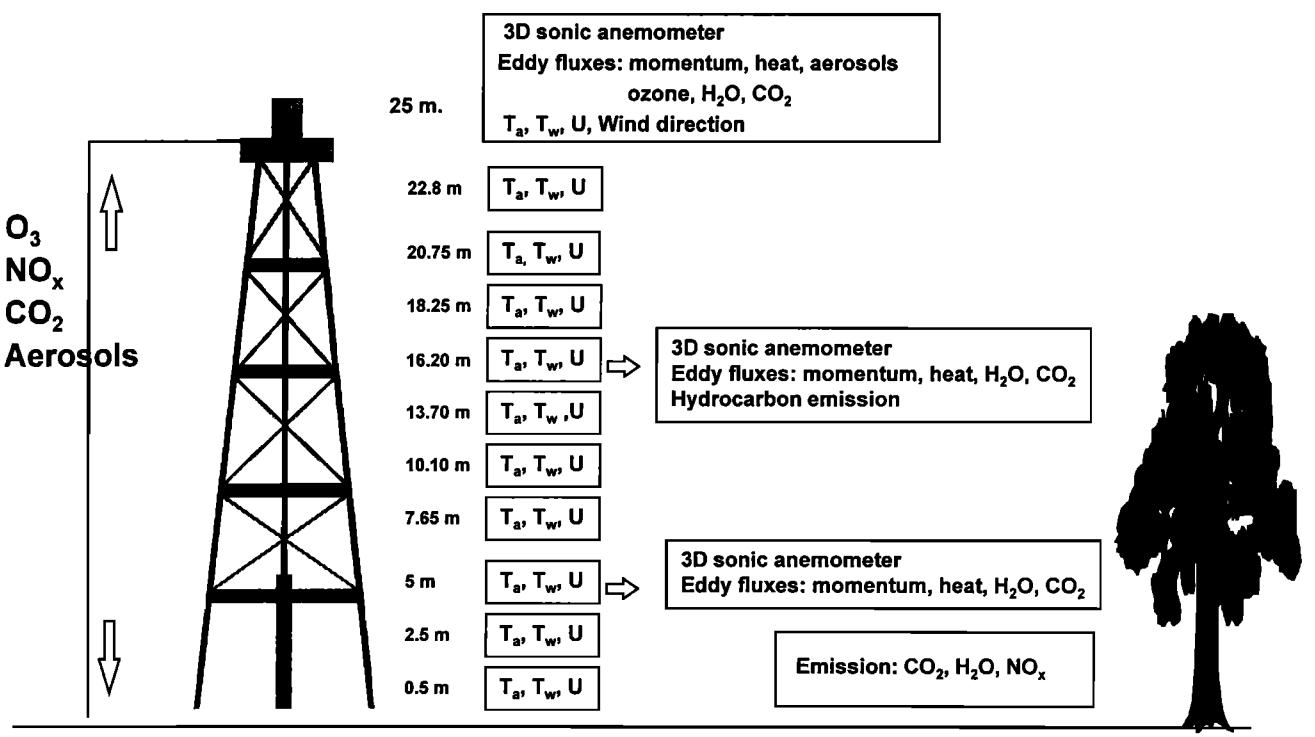

Figure 1. Experimental setup.

cent device [*Güsten et al.*, 1992], with a response time better than 0.1 s and a detection limit lower than 50 ppt. The aerosol analyzer, developed at the laboratory by *El Bakkali* [1991], is based on an electrical principle. The aerosol particles are electrically charged by a unipolar charge obtained by Corona effect, and the resulting current is measured. The flow rate (2.5 l s^{-1}) is high enough for the statistical fluctuations to be negligible. The time constant is about 0.2 s. For a lognormal particle size distribution (geometrical mean $\approx$ 0.04 μm, standard deviation $\approx$ 2.5) representative of the experimental distribution obtained earlier at a similar site, the analyzer has a response centered at 0.15 μm, with the same standard deviation; 90% of the detected particles have a size between 0.05 and 1 μm.

5. Emission or absorption of the following compounds: nitrogen oxides (using dynamic chambers on the ground, as described by *Serça et al.* [1994]), hydrocarbons (using bags, as described by *Clément et al.* [1993]), CO_2, and water vapor (ventilated chambers on the ground surface).

3. Climatic Conditions and Canopy Microclimate

The experiment was conducted from June 9 to June 22, 1992. The climatic conditions encountered during this period were characterized by frequent rains and rather low wind.

During the measurement campaign the average daily temperature at 25 m varied between 13° and 21°C . The nocturnal minima measured at z = 0.5 m ranged between 5 and 15°C, and the daytime maxima varied between 14° and 28°C (Figure 2a). The daily thermal amplitudes were relatively large, of the order of 10°-15°C, except for June 9, 10, 11, 21, and 22, where they were much lower (Figure 2a). On these days solar radiation was very low (Figure 2b), whereas at this time of the year it normally peaks at about 900 W m^{-2}. It can be seen that the sky was cloudless on one day only (June 18). The other days were characterized by partly cloudy skies. The soil was well watered. At this time of the year, evaporation rates were rather large, as can be inferred from Figures 10 and 12 ($\approx$ 300-400 W m^{-2}).

Wind directions (Figure 2c) were indicative of west and northwest regimes principally, rather well stabilized at the beginning of the campaign (from June 9 to 12). For June 14, 15, and 16, northeast winds were frequently observed. From June 16 onward the wind regimes were less well defined. Horizontal wind velocity was low during the campaign, with values ranging between 1 and 4 m s^{-1} at 25 m (Figure 2d).

The mean daily ozone concentrations were around 30 ppb from June 9 to 12, 40 ppb from June 13 to 16, and around 60 ppb from June 19 to 22 (Figure 3a). The first of these periods corresponds to west or northwest winds, low radiation, and a low level of pollution, as indicated by the value of aerosols and nitrogen oxides. Maximun ozone values higher than 70 ppb were recorded on June 17 and 18. A characteristic daily variation is observed over most days, with a decrease in concentration during the nocturnal period, an increase after sunrise, and a maximum in the middle of the day. In a few cases, sudden variations of ozone were observed in correlation with variations of aerosol and nitrogen oxides, possibly indicating a local contamination of the site.

The concentration in aerosols was generally less than 10,000 particles per cm^3 (Figure 3b). The highest values were recorded during the period June 14-16, when the site

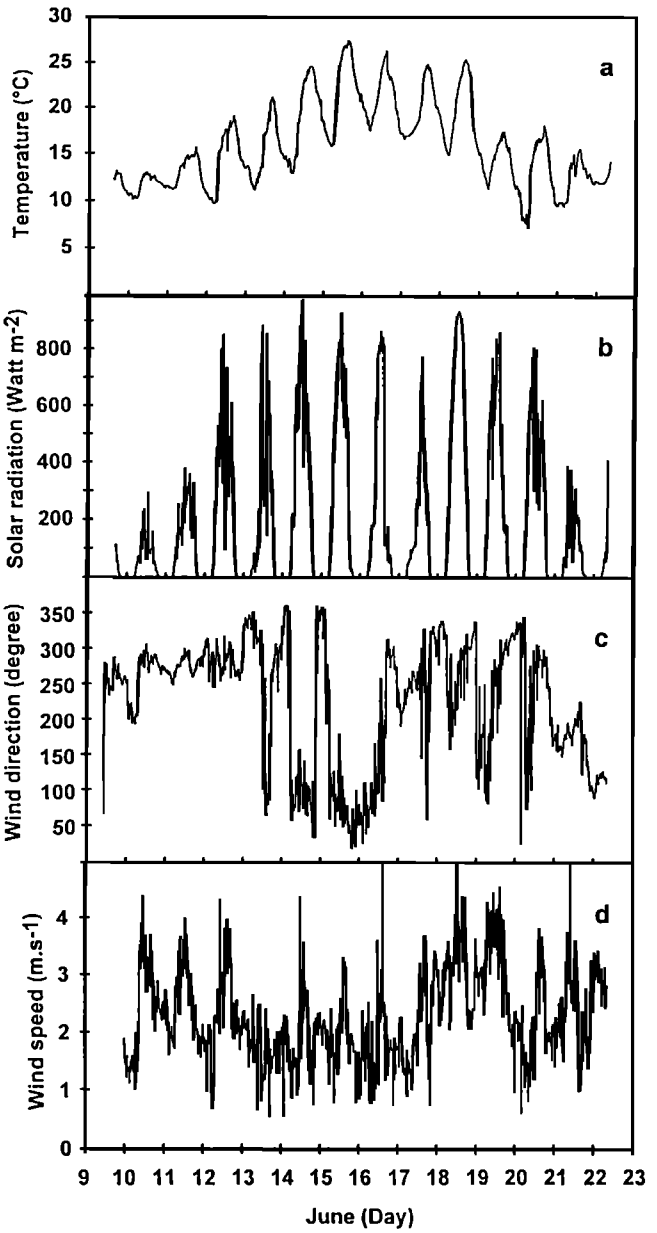

Figure 2. Mean meteorological parameters, from June 9 to June 22, 1992: (a) mean air temperature at 25 m, (b) global radiation, (c) mean wind direction, (d) mean horizontal wind velocity at 25 m.

was under northeast winds, i.e., coming from the urban area of Bordeaux.

The average concentration in nitrogen oxides was normally between 2 and 10 ppb, except during a few pollution periods, when levels of 30 ppb were recorded (Figure 3c). The CO_2 concentration measured above the forest varied between 350 and 420 ppm with, as expected, a minimum in the middle of the day and a maximun during the nocturnal period (Figure 3d).

4. Spectral and Cospectral Analysis of Turbulent Data

The power spectra of turbulent variables (vertical wind velocity and scalars: temperature, humidity, concentrations in carbon dioxide, ozone, and aerosol particles) and the cospectra of vertical velocity and all scalars were computed

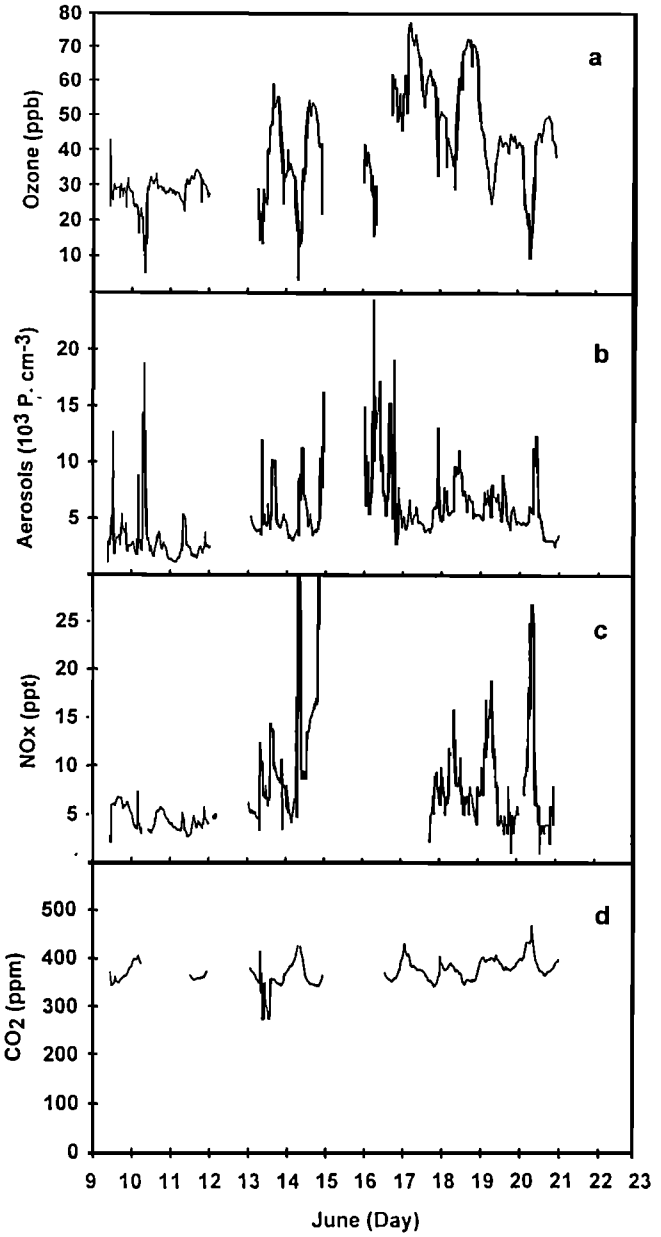

Figure 3. Mean concentrations at 25 m, from June 9 to June 22, 1992: (a) ozone, (b) aerosol particles, (c) nitrogen oxides, (d) CO_2.

at height z = 25 m. Because the turbulent variables were acquired on different systems at different frequencies, various treatments were performed. Spectra and cospectra shown here were obtained from time series of 2^{13} points, tapered with a cosine bell function. To reach low enough frequencies, to which special attention is paid further, the number of points was first reduced in the high-frequency range by block averaging the original time series, using unweighted, nonoverlapping blocks of length between 0.1 and 0.3 s. For the sake of clarity, all spectra and cospectra were subsequently band averaged. In some cases, several spectra from contiguous time series were also averaged. In what follows, the spectral and cospectral densities ($S_{xx}(f)$ and $S_{xy}(f)$, respectively) are frequency weighted and normalized by the corresponding variances ($fS_{xx}(f)/\sigma_x^2$ and $fS_{xy}(f)/(\sigma_x\sigma_y)$). We can then directly compare the results obtained with data that may exhibit considerable differences in variances or covariances. All results are plotted against the dimensionless frequency $n = f(z-d)/U(z)$, which is the appropriate scaling for the atmospheric surface layer. The displacement height d was calculated from a series of in-canopy mean horizontal velocity profiles, using the method described by *Thom* [1971]. A mean value d = 11 m (or d/h = 0.71) was found.

Figure 4 shows the spectra of w, T, H_2O, CO_2, O_3, and aerosol particles, averaged over the period 1015-1215 UT on June 18, which was the clearest day of the experiment. At that time, mean wind speed was about 3.5 m s^{-1}, with slightly unstable atmospheric conditions. The w spectrum exhibits a familiar pattern. It peaks at a normalized frequency of $n \approx 0.2$ and shows an inertial subrange spanning over about one and a half decade with the expected -2/3 slope. On the low-frequency side it decreases monotonously. These results are all in good agreement with the features usually observed in the atmospheric surface layer (see *Kaimal and Finnigan* [1993] for a review). All scalar spectra exhibit the same features in the energy-containing range where they peak at a slightly lower frequency ($n \approx 0.10$-0.15) and also in the inertial subrange where they also fit well with the Kolmogorov theory.

The corresponding cospectra are displayed in Figure 5 in area-preserving form (with a minus sign for CO_2, O_3, and aerosol particles). Here again we observe a very good spectral collapse over the whole frequency range, apart from some unavoidable noise which occasionally affects the curves. The cospectra peak around n = 0.1 ($f \approx 0.025$ Hz at that height and for these particular runs). This is very consistent with the value of 0.03 Hz found by *Collineau and Brunet* [1993] for the mean gust frequency in this forest, using a wavelet-based detection scheme for the detection of coherent structures in turbulent time series. In all cases, most of the transfer occurs in a spectral band between n = 0.04 and n = 0.4 (f between 0.01 Hz and 0.1 Hz) and no flux is transported beyond $n \approx 4$ ($f \approx 1$ Hz). When plotted in a log-log form (not shown here), all cospectra exhibit the expected -4/3 slope over one and a half decade.

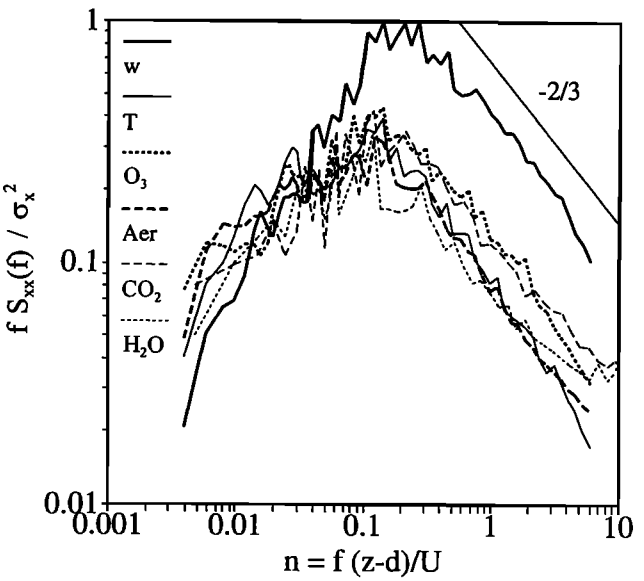

Figure 4. Normalized, frequency-weighted spectra for vertical velocity and scalars (June 18, 1015-1215 UT).

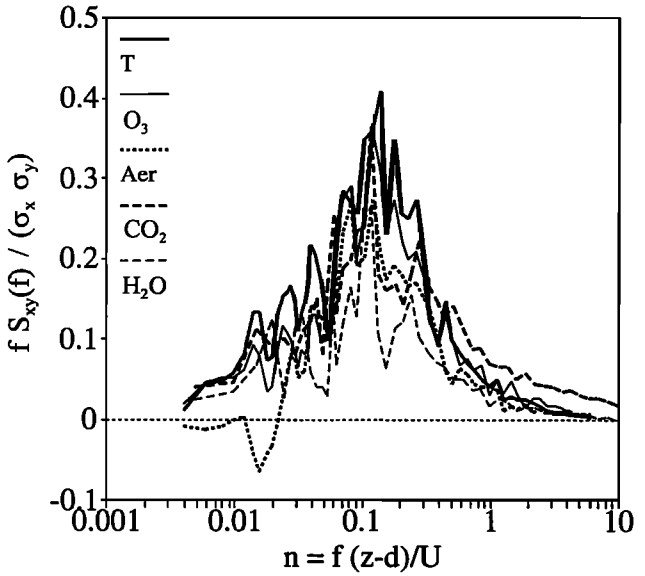

Figure 5. Normalized, frequency-weighted cospectra for all scalar fluxes (June 18, 1015-1215 UT).

On the low-frequency side, most cospectra show a continuous decrease and are nearly closed at the lowest resolved frequency. In other words, the corresponding integration time has allowed us to capture all the scales responsible for vertical turbulent fluxes. In the case of aerosol particles however, the cospectrum shows extra energy at low frequencies, with a sign reversal. In other words, we observe a positive correlation between the vertical wind speed and the concentration in aerosol particles at timescales larger than 3 min. At such timescales this correlation is very unlikely to be due to vertical turbulent transfer associated to the dry deposition, given the typical scales of motion observed over this forest [*Collineau and Brunet*, 1993].

In the present case this low-frequency behavior is of little importance since the associated flux fraction is negligible. However, our attention was drawn in this experiment to frequent, unexpected features in the daily evolution of all scalar fluxes, calculated over periods of the order of 15-30 min (very high run-to-run variability, sign reversals ...). A close look at this problem showed that these features were systematically associated with spurious spectral patterns at low frequencies, which will be the object of section 5.

5. Low-Frequency Distortions

The averaged spectra of vertical velocity and scalars obtained on June 16 from 1300 to 1330 UT are displayed in Figure 6. When compared to Figure 4, all spectra exhibit extra energy between $n \approx 0.01$ and $n \approx 0.03$, at frequencies which differ significantly from those associated with the energy-containing range. In most cases the main peak mentioned above is not visible. The spectral densities of CO_2, O_3, and aerosol particles also exhibit a minimum between $n \approx 0.02$ and $n \approx 0.07$. Beyond $n \approx 0.1$ the spectral shapes are similar to those in Figure 4, although they look different; here this is simply due to the normalization by the variances, which are increased by the extra energy at low frequencies. Another type of representation allows us to highlight the low-frequency behavior. It consists of first multiplying all frequency-weighted spectral densities $fS_{xx}(f)$ by $f^{3/2}$; the resulting densities are then normalized by their mean value $[f^{5/2}S_{xx}(f)]$ over the inertial subrange (here, between $n = 0.7$ and $n = 8$). This treatment makes the inertial part of the spectra appear as a horizontal line around a mean value of 1 and dilates the range of variation in the low frequencies. The results are shown for the mean spectra of Figure 4 (June 18) and for the same set of 30-min spectra as in Figure 6 (June 16, 1300-1330 UT). It is clear that in the first case (Figure 7a), all spectral densities increase with frequency smoothly and in a consistent manner, up to the inertial subrange represented as a plateau. On June 16 (Figure 7b) the low-frequency behavior is much more erratic. It also turns out to be quite variable from run to run.

Turning now to the cospectra (Figure 8), it appears that the low frequencies visible on the individual scalar spectra may be correlated with vertical velocity. Indeed, we observe dramatic low frequency distortions which appear under various forms such as large-magnitude peaks (e.g., all cospectra in Figure 8) or reversals in sign (visible in later runs). Sometimes the main peak directly associated with vertical turbulent transfer is entirely masked by extra low-frequency energy. These features may have considerable consequences on the mean fluxes, when directly computed from the raw data. Depending on the sign and the importance of the low-frequency contributions, the fluxes may indeed be overestimated or underestimated. Also, erratic features or occasional large peaks may appear in time series of all mean scalar fluxes, that cannot be explained on any other ground. We even happened to obtain fluxes with a wrong sign. It is particularly illustrative to consider the sum of sensible and latent heat fluxes (H and LE, respectively), since it can be compared to an objective reference, the available energy (or at least the net radiation Rn). Figure 9 shows both $H + LE$ and Rn on June 16. In the early morning and in the midafternoon the agreement is quite good, the difference being of the order of the heat storage, that we did not evaluate here but which was shown to be typically about 50 W m^{-2} in the midmorning and 10-15

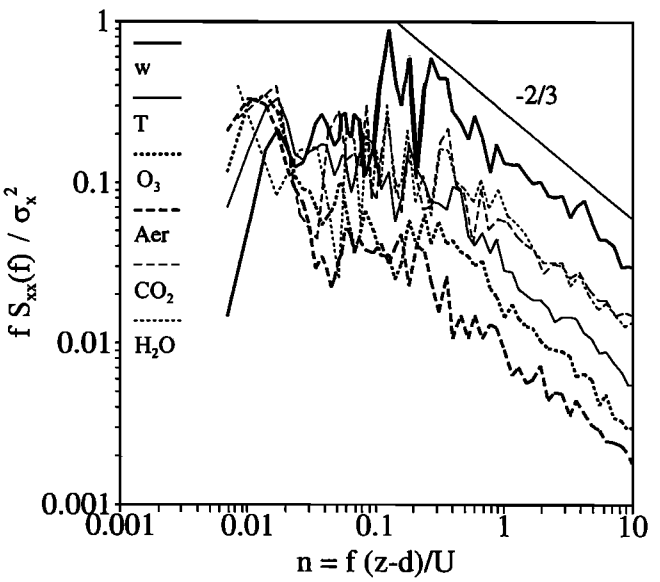

Figure 6. Normalized, frequency-weighted spectra for vertical velocity and scalars (June 16, 1300-1330 UT).

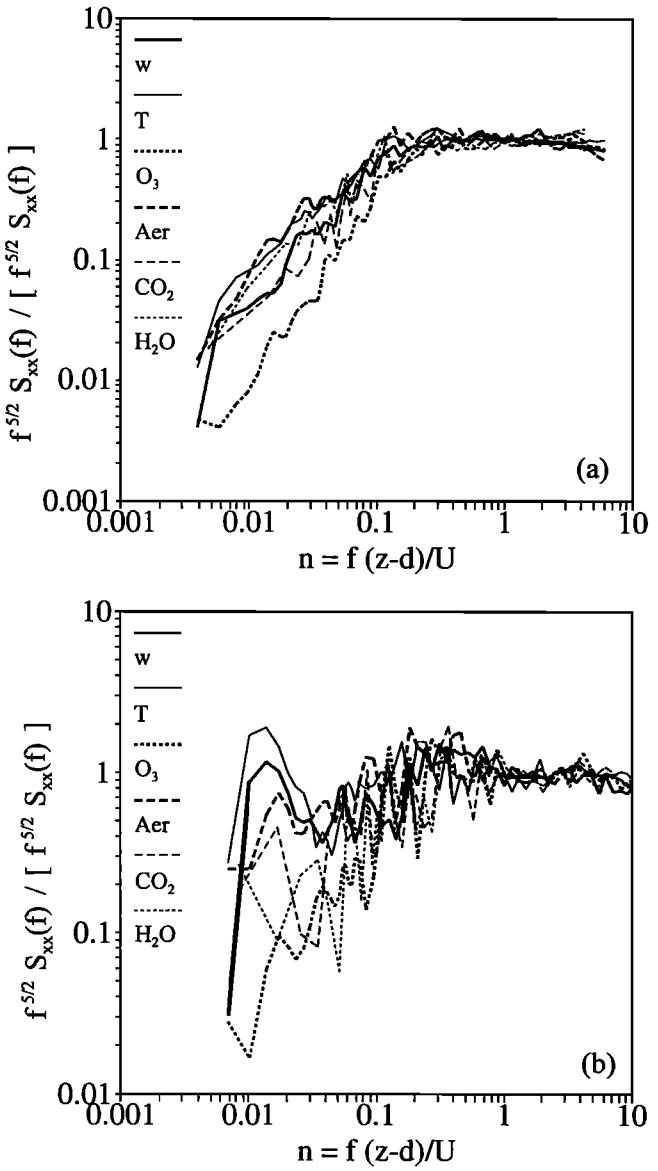

Figure 7. Frequency-weighted spectra for vertical velocity and scalars, multiplied by $f^{3/2}$ and normalized by the corresponding averaged value (in brackets) in the inertial subrange (see text). (a) June 18, 1015-1215 UT; (b) June 16, 1300-1330 UT.

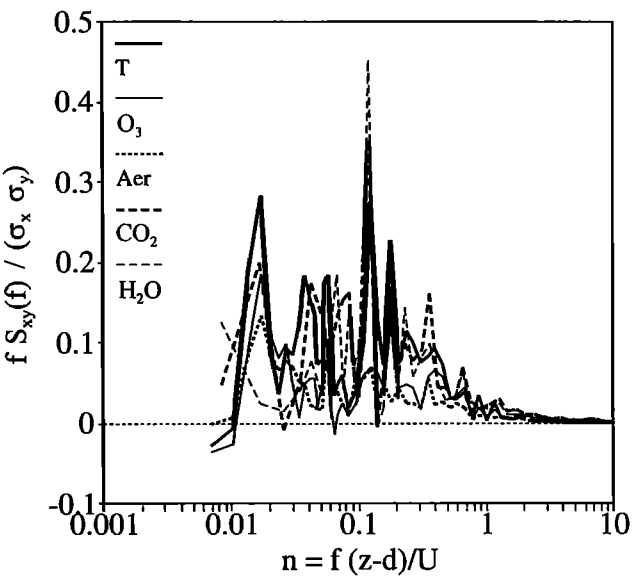

Figure 8. Normalized, frequency-weighted cospectra for all scalar fluxes (June 16, 1300-1330 UT).

W m^{-2} in the afternoon, at the same site and under similar meteorological conditions [*Diawara et al.*, 1991]. However, between 1030 and 1430 UT, large discrepancies appear: for example, *Rn-(H+LE)* is about +300 W m^{-2} at 1100 UT and -200 W m^{-2} at 1300 UT (the run corresponding to the cospectra shown in Figure 8).

The reasons for the presence of low frequencies are not quite clear. They have been observed to be more important in the case of ozone, carbon dioxide, and aerosol particles than for temperature or specific humidity. Such phenomena were observed in this experiment on most days with unstable weather, i.e., frequent cloud passes or often changing wind direction. They are obviously due to the presence of slow trends (frequency components with a period longer than the record length, or of the same order) in the time series. These nonstationary events may be associated with factors such as background "pollution" or heterogeneities in the distribution of sources and sinks, combined with large-scale advective motions due to boundary-layer-type structures.

Whatever this may be, it becomes obvious that turbulent fluxes must not be computed "blindly." The simple observation of time changes in the mean concentration *dC/dt* is not sufficient for detecting detrimental low-frequency trends, for several reasons. Firstly, one cannot properly define a mean value from time series exhibiting significant low frequencies, since stationarity at the scale of the integration period is a prerequisite; consequently, the estimation of time or spatial derivatives is not, strictly speaking, possible. Secondly, examination of data on this basis would certainly lead to many wrong rejections and acceptances: on the one hand, since scalar concentration and vertical velocity have to

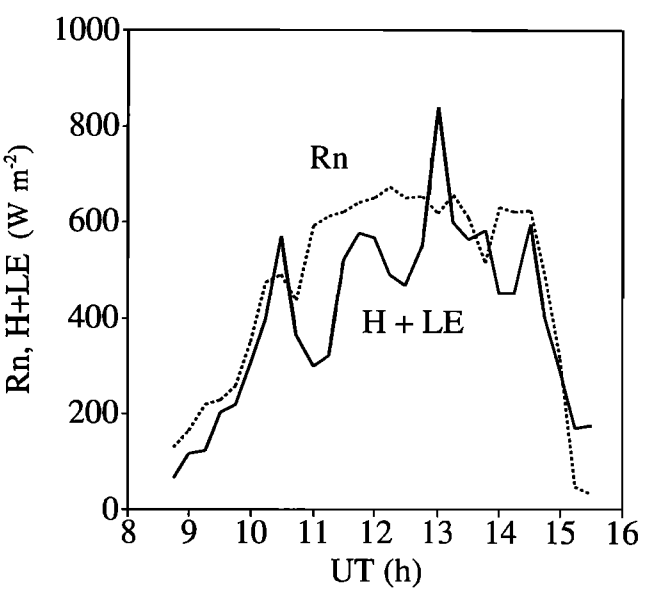

Figure 9. Comparison of net radiation (*Rn*) with the sum of sensible (*H*) and latent (*LE*) heat fluxes, June 16.

be correlated at low frequencies to really cause problems, large values of dC/dt alone may have little or no effect on the covariance. On the other hand, we have observed that one can have both small values of dC/dt at the scale of the integration period and significant correlation at slightly smaller timescales, leading to biased flux estimates. A consequence of this is that only part of the problem is addressed by examining the full conservation equation, including advection and diffusion terms, as *Wesely et al.* [1985] did. The flux errors evaluated by their method for the data of June 16 are much smaller than the discrepancies observable in Figure 9, given the microclimatic conditions then prevailing. It must be made clear that the problems addressed here occur at timescales both shorter than the integration period and larger than the timescales associated with vertical turbulent transfer. In this particular forest canopy the transport of material by large-scale gusts occur on timescales of 30 s only [*Collineau and Brunet*, 1993] and very little flux is transferred by motions with timescales longer than 2-3 min.

Even if this is very demanding and time consuming, one should therefore always look at the spectral and cospectral behaviors of the relevant turbulent variables. If significant energy is found at low frequencies, it may be possible in some cases to filter out the latter. For this, several possibilities exist. Filtering may be performed (1) in the Fourier space, using more or less sharp filters; (2) on the raw digital data, using least squares methods to remove linear or polynomial trends, or using weighted running means of finite width; or (3) on line, with recursive techniques such as the popular RC filter [*McMillen*, 1988]. However, caution must be exercised if such techniques are to be applied. First of all, filtering can be performed only if the relevant cospectral regions are well separated, which is not the case for the examples presented in Figure 8. It is worth mentioning here that low-frequency distortions are likely to be all the more detrimental as the observation level is higher, mean wind speed lower and instability greater. In the present case, the normalized frequency of the cospectral peak ($n \approx 0.03$) corresponds to a timescale of the order of 30 s, whereas over an agricultural field (e.g., $z\text{-}d = 2$ m) with higher wind velocity (e.g., $U = 6$ m s^{-1}) the corresponding timescale would be 1 order of magnitude smaller (3 s). In other words, the cospectra in the latter case may be shifted enough to higher frequencies for a gap to exist with the spectral range "polluted" by the low-frequency contributions, given the timescales at which they are observed (typically, a few minutes). Secondly, all filters have their own drawbacks. For instance, the spectral response of an equally weighted running mean has several rejection bands at high frequencies, some of them being in phase opposition with the original spectra; this may cause spurious effects in particular cases. Also, the RC filter introduces a lagged moving average, which may be detrimental to the covariance calculations. Moreover, it does not satisfy Reynolds averaging rules [*Kaimal and Finnigan*, 1993].

We feel that the problems associated with the existence of low-frequency distorsions have been underestimated in the past. The growing availability of fast-response sensors has permitted much progress in field measurements but may also have led us to use eddy correlation systems as black boxes. Clearly, this should not be the case and further work on the problems raised here is required. Furthermore, these low frequencies also result in temporal variations of the scalar profiles so that the vertical gradients are then not directly linked with the surface flux. For instance, it was observed under such circumstances that the aerosol gradient sometimes oscillates between positive and negative values. The resulting mean profile may lead to wrong estimations of dry deposition (or emission) of the relevant scalar. With the aerodynamic method, separation between the low frequencies and those responsible for the vertical turbulent transfer is never possible.

6. Diurnal Fluxes and Deposition Velocity Variations

We now present results obtained over two days (June 14 and 18) on the diurnal evolution of the ozone and aerosol fluxes. These two days exhibit marked differences in the meteorological conditions (Figure 2). June 18 is a fine, pollution-free day with a smooth evolution of global radiation, a mean wind speed of the order of 3-4 m s^{-1}, and a mean wind direction indicating a westerly regime. June 14 is characterized by frequent cloud passes and lighter, easterly winds.

The covariances $\overline{w'c'}$, where c' is the concentration in ozone or aerosol particles, are computed after the raw data are rotated to align the sonic anemometers in the mean wind direction, over integration periods of 15 min. For each run, spectra and cospectra are examined. When low frequencies are apparent and cannot be separated from the active region, the runs are discarded. Otherwise, the data are high-pass filtered in the Fourier space, using a cutoff frequency adapted to each case. The dry deposition velocity is then computed as

$$v_d = -\overline{w'c'}/C \,, \qquad (1)$$

where C is the concentration in ozone or aerosol particles at 25 m.

On June 18 the measurements were performed from 1000 to 2030 UT. Net radiation Rn (Figure 10) shows a smooth temporal evolution with a maximum value of about 700 W m^{-2} around 1200 UT. The friction velocity u_* (Figure 10) oscillates around 0.6 m s^{-1} and drops in the late afternoon, down to 0.3 m s^{-1} at the inversion time (1800 UT), following a drop in mean wind speed U from 3.5 to 2 m s^{-1}. The ozone concentration exhibits little variation throughout the day, remaining between 50 and 60 ppb with a maximum around 1500 UT. The dry deposition velocity of ozone (Figure 11) varies in the same way as net radiation (and sensible and latent heat fluxes, which both exhibit similar trends). It has a maximum value of about 0.7 cm s^{-1} between 1000 and 1200 UT and gradually decreases in the afternoon to a value of about 0.1 cm s^{-1} reached after the inversion time. The concentration in aerosol particles exhibits little variation too, decreasing slowly from 9000 (1200 UT) to 7000 (2000 UT) particles cm^{-3}. The dry deposition velocity (Figure 11) has a similar variation to that for ozone, although it decreases more slowly in the afternoon. It also varies from about 0.7 cm s^{-1} around midday to 0.1 cm s^{-1} at night. As has already been reported in several studies [e.g., *Wesely et al.*, 1985], this illustrates the difficulty of sorting out the various factors influencing the deposition of different species, as many fluxes exhibit striking similarities on a

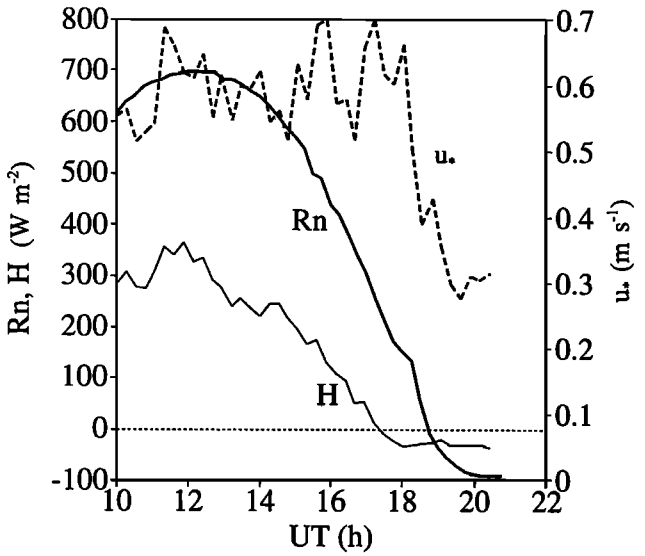

Figure 10. Daytime variation of net radiation, sensible heat flux, and friction velocity, June 18.

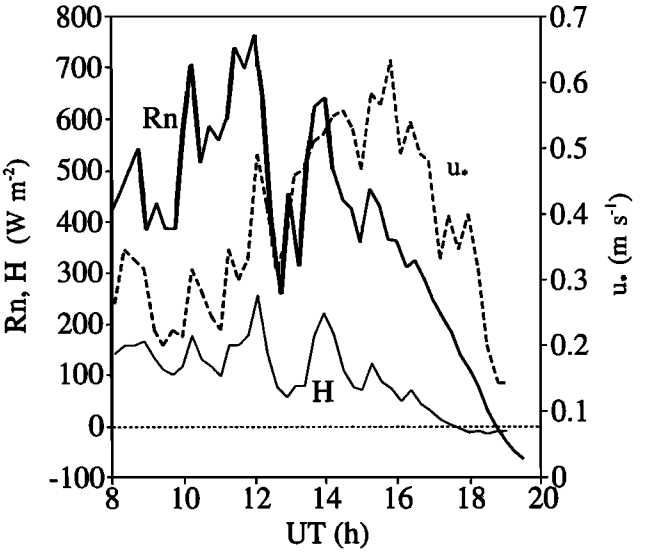

Figure 12. Daytime variation of net radiation, sensible heat flux, and friction velocity, June 14.

diurnal or hourly basis, even though the responsible mechanisms are quite different. The values of both deposition velocities are in good agreement with other studies [*Hosker and Lindberg*, 1982; *Hicks et al.*, 1982, 1987; *Wesely et al.*, 1983, 1985]. In particular, values as high as 0.7 or 0.8 cm s^{-1} have been oberved for the deposition velocity of fine particles over a deciduous forest [*Wesely et al.*, 1983] or grass [*Wesely et al.*, 1985].

On June 14 the measurements were performed from 0800 UT to 1930 UT. Net radiation is much more perturbed than on June 18, because of cloud passes (Figure 12). The friction velocity follows the mean wind speed; it gradually increases from 0.2 m s^{-1} in the morning to 0.55 m s^{-1} around 1500-1600 UT, then decreases relatively rapidly to 0.15 m s^{-1} (Figure 12). The concentrations in ozone and aerosol particles show a larger range of variation than in the previous case. The ozone concentration increases from 20 ppb at 0800 UT to 60 ppb at 1200 UT and later decreases slowly down to 40 ppb. The concentration in aerosol particles varies between 7000 and 4000 particles cm^{-3}, with a minimum in the midafternoon. Again, the temporal variation in the dry deposition velocities for ozone (Figure 13) resembles that of net radiation. In particular, the two peaks followed by sharp drops at 1200 and 1400 UT are quite visible. They are also apparent on the dry deposition velocity of aerosol particles (Figure 13). However, in the afternoon the friction velocity also decreases. Both deposition veloc-

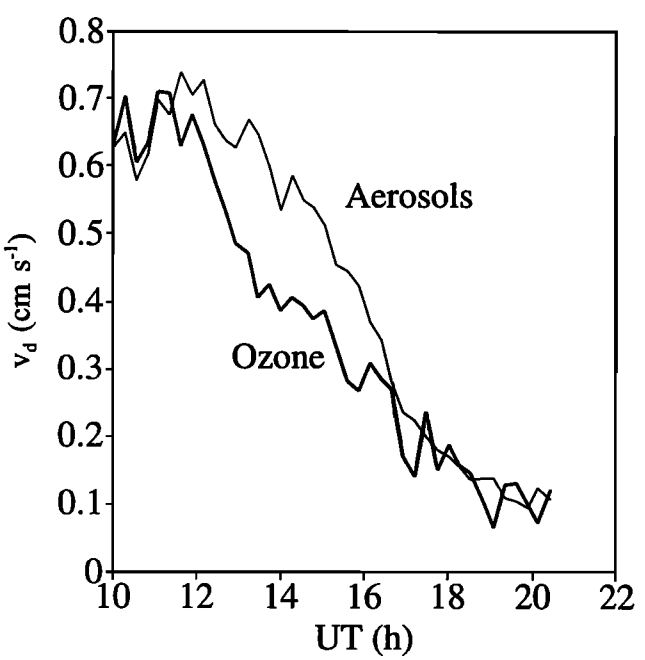

Figure 11. Daytime variation of dry deposition velocities for ozone and aerosol particles, June 18.

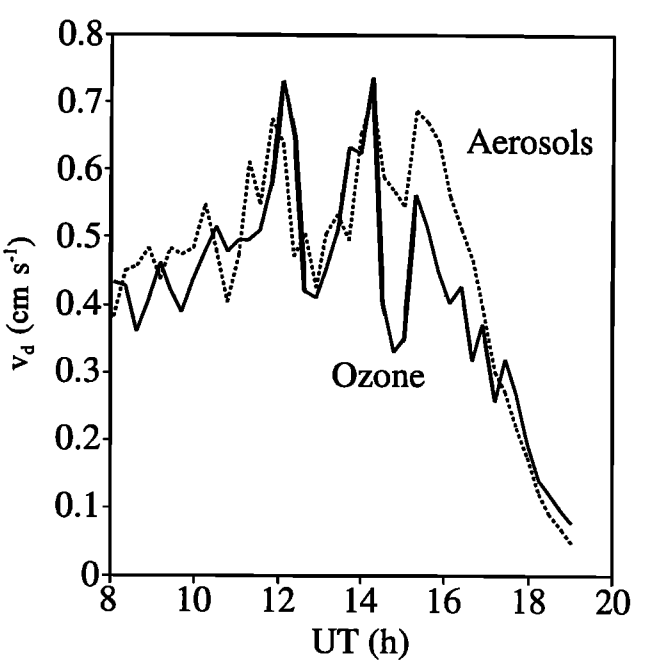

Figure 13. Daytime variation of dry deposition velocities for ozone and aerosol particles, June 14.

ities oscillate between 0.4 and 0.7 cm s^{-1} until about 1500 UT, before decreasing down to 0.1 cm s^{-1}.

Although a detailed study of the underlying mechanisms is beyond the scope of this paper, we can analyze these results in a conventional way, using the standard "big-leaf" multiple resistance model. In this framework the dry deposition velocity is expressed as

$$v_d = (r_a + r_b + r_c)^{-1} , \quad (2)$$

where r_a is the aerodynamic resistance for the species of interest, r_b a resistance accounting for bluff body effects, and r_c a composite canopy resistance depending, among other factors, on the stomatal resistance of the leaves (see, for example, *Hicks et al.* [1987]). The cases of ozone and aerosol particles have to be considered separately, because ozone deposition is known to be stomatally controlled, whereas aerosol deposition is not, and also because the resistances r_b are likely to be different (see below).

Let us first consider the case of ozone. The aerodynamic resistance can be conveniently evaluated as

$$r_a = U(z) / u_*^2 . \quad (3)$$

This is true in stable and near-neutral conditions, but in unstable conditions this amounts to neglecting the differences in stability corrections between momentum and scalars. However, this approximation turns out to be much better than trying to evaluate r_a from the surface layer log-law, since our measurement level is well within the roughness sublayer. It has been shown that quite large errors can be made when ignoring this [*Cellier and Brunet*, 1992]. The values found for r_a are of the order of 5-20 s m^{-1}. The "excess" resistance r_b is usually introduced because the resistance to mass and energy transfer differs from that for momentum (see, for instance, *Garratt and Hicks* [1973], *Brutsaert* [1982], and *Hicks et al.* [1987]). Close to the exchange surfaces, mass and energy transfer is controlled by molecular processes in the leaf laminar boundary layers, whereas momentum is mainly transferred by pressure forces, responsible for the so-called "bluff body" effects. We can express r_b as

$$r_b = (u_* B)^{-1} (Sc/Pr)^n , \quad (4)$$

where B is the inverse Stanton number [*Owen and Thompson*, 1963], Sc the Schmidt number for the scalar under consideration (1.07 for ozone), and Pr the turbulent Prandtl number (0.72). The presence of the latter accounts for the fact that most basic studies on B have been conducted on heat transfer. The exponent n is not rigorously known but seems to be close to 2/3 for most gases. Assuming that the value $B^{-1} \approx 3/k$ ($k \approx 0.4$ being the von Karman constant) obtained for heat transfer by *Lagouarde et al.* [1993] in a separate study over the same forest canopy is also valid for ozone, equation (4) then reduces to $r_b \approx 10/u_*$. Consequently, r_b lies between 15 and 30 s m^{-1} most of the time. We can now evaluate the uptake resistance r_c for ozone (or its inverse $g_c = 1/r_c$, a "surface conductance" for ozone), as the remaining term in equation (2). Figure 14 shows the ozone deposition velocity v_d, along with $g_c = (v_d^{-1} - r_a - r_b)^{-1}$. It can be seen that r_a and r_b play a minor role, the deposition

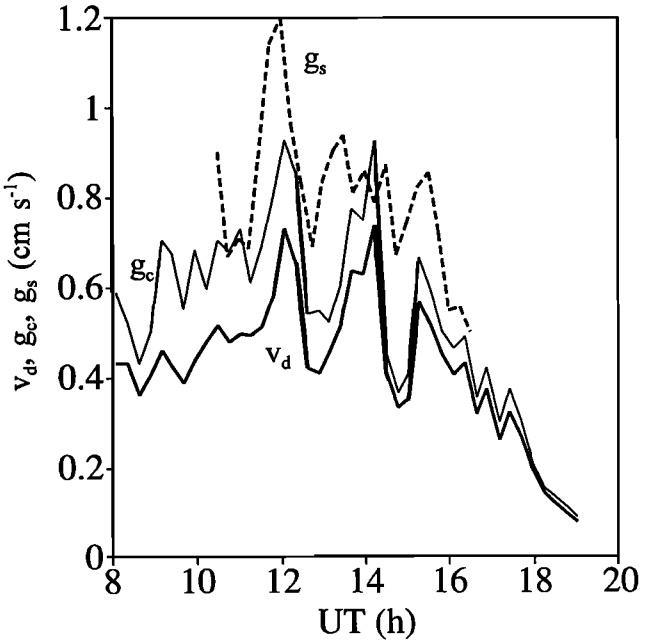

Figure 14. Daytime variation of the ozone deposition velocity (v_d), ozone "uptake conductance" (g_c), and surface conductance for water vapor (g_s), June 14.

of ozone being mostly dictated by r_c. In the same figure we have also plotted the bulk surface conductance for water vapor g_s, which reflects to a large extent the stomatal conductance of the leaves. The calculation of g_s implies using equation (1) with an opposite sign, and assuming that the surface concentration corresponds to the saturation vapor pressure at the bulk canopy temperature. This amounts to deducing g_s from a Penman-Monteith equation at the canopy scale, using measured values of the evapotranspiration flux. It can be seen that the conductances g_c and g_s appear highly correlated and of the same order of magnitude, confirming that ozone deposition is mainly controlled by stomatal opening.

The deposition mechanisms for aerosol particles are still largely unknown. Ignoring the surface resistance r_c in equation (2), the deposition velocity can be simply written as $v_d = (r_a + r_b)^{-1}$. However, use of equation (4) for r_b is subject to large uncertainties regarding B and n. As the Schmidt number for particles of radius 0.05-1 μm is 4 to 6 orders of magnitude larger than for a gaseous species [*Hicks et al.*, 1987], use of $B^{-1} = 3/k$ and $n = 2/3$ as for ozone would lead to very high values for r_b, incompatible with the observed deposition velocities. This has been repeatedly mentioned when dealing with real-world plant canopies, especially over forests, whereas wind-tunnel measurements provide much lower deposition velocities for fine particles [*Hicks et al.*, 1982, 1987; *Wesely et al.*, 1983]. In the present state of knowledge regarding particle deposition to vegetation, it has been argued by several authors [e.g., *Wesely et al.*, 1983, 1985; *Hicks et al.*, 1987] that following purely empirical approaches, as an interim procedure, was probably the best thing to do.

In this context, *Wesely et al.* [1985] found that the deposition velocity of sulfate particles, once normalized by friction velocity, was primarily dependent on the Monin-Obukhov length scale L. Plotting v_d/u_* versus $1/L$, they

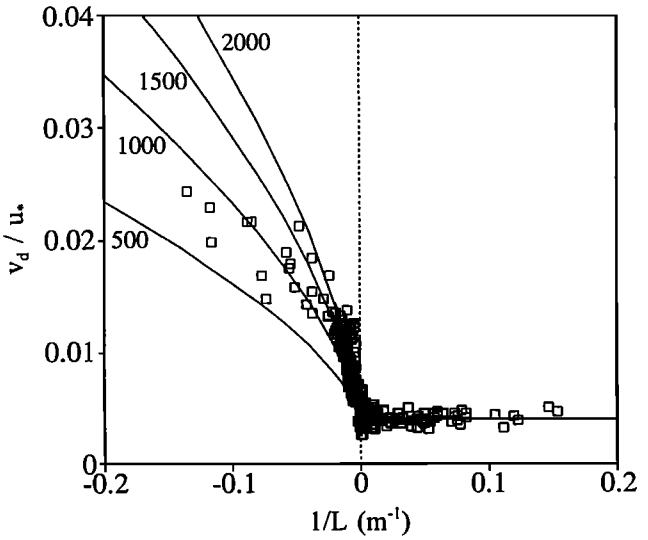

Figure 15. Normalized deposition velocity for aerosol particles versus the inverse of the Monin-Obukhov length (all data from June 14, 15, 16, 18, 19). The solid curves correspond to equation (6) with $a = 0.004$ and $b = 0.0009$, for various values of the planetary boundary layer height z_i (appearing in the left-hand side of the figure and expressed in meters).

found that in near-neutral and stable conditions, v_d/u_* remains fairly constant around a value of 0.002. In unstable conditions, v_d/u_* increases with increasing instability and they showed that their data could be reasonably well represented by a parametric form, which we can rewrite as

$$v_d/u_* = a + b\,(z_i/L)^{-2/3}, \qquad (5)$$

with $a = 0.002$ and $b = 0.0009$; z_i is the planetary boundary layer height, as deduced from acoustic sounder measurements. Figure 15 shows a similar plot of our own data, using the 210 values collected on June 14, 15, 16, 18 and 19. Our results appear very similar to those of *Wesely et al.* [1985], at least from a qualitative point of view. In near-neutral and stable conditions, v_d also appears as proportional to u_*, with a coefficient of 0.004. The reason why we obtain over our pine forest a value twice as much as that obtained by *Wesely et al.* [1985] over a grassy surface is unclear. The ratio v_d/u_* increases with increasing instability, reaching about 0.025 for the most unstable data ($L \approx 7$ m). We cannot test equation (5) because no measurements of boundary layer height were performed in our experiment. However, we have plotted equation (5) in Figure 15 for four values of z_i (500, 1000, 1500, and 2000 m), keeping $b = 0.0009$ but taking $a = 0.004$ which better fits our observations. The simulated variation is quite compatible with the experimental data. Indeed, the points corresponding to small values of $1/L$ were obtained after 1200 UT, i.e., when the boundary layer already had substantially grown. Also, most of the data with $1/L \leq -0.03$ were recorded in the morning of June 14. This of course does not prove that our results can be represented by equation (5) but constitutes a mere indication that this type of parameterization may represent some underlying mechanism. The rationale behind such a scheme can be exposed along the following lines. The variance of horizontal wind speed, partly caused by convective motions in the atmospheric boundary layer, has been shown to remain approximately constant in the surface layer and to be a function of z_i/L rather than z/L, contrary to the variance of vertical velocity [*Panofsky et al.*, 1977]. The increase with thermal instability of the turbulent kinetic energy associated with the horizontal fluctuations might therefore explain the observed enhancement of the deposition velocity. Clearly, this demands confirmation and the deposition mechanisms of aerosol particles are still largely unknown.

7. Summary and Conclusions

Our experimental results show that low-frequency fluctuations in the concentration of scalars such as ozone or submicronic particles can cause detrimental spectral distorsions, significantly affecting the measurement of dry deposition (or surface source for other scalars). Generally, filtering can be performed to remove these effects, but this is not always the case, especially over forests under low wind velocities. For the sake of safety, spectral analysis should always be performed. The range of values obtained for the dry deposition velocities of ozone and aerosol particles in the range 0.05-1 μm were found to be in good agreement with other similar reported studies. Their diurnal variations are broadly consistent with the present knowledge on the determinism of dry deposition. They suggest that the surface uptake resistance (mainly stomatal) is the limiting factor governing O_3 deposition, whereas the deposition of aerosol particles may be rather controlled by dynamical and convective processes. In the former case, a striking similarity was obtained between the ozone uptake resistance and the bulk stomatal resistance, using estimates of the other resistances involved; in the latter case, the deposition velocity was found, as in other published studies, to be much larger than the values predicted by classical laminar boundary layer calculations and to depend on atmospheric instability. Further work is required to predict quantitatively the deposition velocities and uptake rates. The present data set as well as future planned experiments will be used for this purpose.

Acknowledgments. This study was supported by the French CNRS "Programme Environnement" through the "Phase atmosphérique des cycles biogéochimiques" subprogram. We wish to acknowledge the helpful comments and suggestions made by the reviewers.

References

Brutsaert, W., Evaporation into the atmosphere: Theory, history and applications, 299 pp., D. Reidel, Norwell, Mass., 1982.

Cellier, P., and Y. Brunet, Flux-gradient relationships above tall plant canopies, *Agric. For. Meteorol., 58*, 93-117, 1992.

Clément, B., M.-L. Riba, V. Simon, and L. Torres, Automatic determination of monoterpenes in forested area, *Int. J. Anal. Chem., 50*, 19-27, 1993.

Collineau, S., and Y. Brunet, Detection of turbulent coherent motions in a forest canopy, II, Time scales and conditional averages, *Boundary Layer Meteorol., 66*, 49-73, 1993.

Diawara, A., D. Loustau, and P. Berbigier, Comparison of two methods for estimating the evaporation of a *Pinus pinaster* (Ait.) stand: Sap flow and energy balance with sensible heat flux measurements by an eddy covariance method, *Agric. For. Meteorol., 54*, 49-66, 1991.

El Bakkali, Y., Etude et réalisation d'un analyseur pour la mesure rapide des fluctuations de l'aérosol atmosphérique, Ph.D. thesis, Univ. Paul Sabatier, Toulouse, France, 1991.

Fontan, J., A. Minga, A. Lopez, and A. Druilhet, Vertical ozone profiles in a pine forest., *Atmos. Environ., 26*, 863-869, 1992.

Garratt, J.R., and B.B. Hicks, Momentum, heat and water vapour transfer to and from natural and artificial surfaces, *Q. J. R. Meteorol. Soc., 99*, 680-687, 1973.

Güsten, H., G. Heinrich, R.W.H. Schmidt, and U. Schurath, A novel ozone sensor for direct eddy flux measurements, *J. Atmos. Chem., 14*, 73-84, 1992.

Hicks, B.B., M.L. Wesely, J.L. Durham, and M.A. Brown, Some direct measurements of atmospheric sulfur fluxes over a pine plantation, *Atmos. Environ., 17*, 2899-2903, 1982.

Hicks, B.B., D.D. Baldocchi, T.P. Meyers, R.P. Hosker, and D.R. Matt, A preliminary multiple resistance routine for deriving dry deposition velocities from measured quantities, *Water Air Soil Pollut., 36*, 311-330, 1987.

Hosker, R.P., and S.E. Lindberg, Review: Atmospheric deposition and plant assimilation of gases and particles, *Atmos. Environ., 16*, 889-910, 1982.

Jambert, C., R. Delmas, L. Labroue, and P. Chassin, Nitrogen compounds emission from fertilized soils in a maize field-pine tree forest agrosystem in the southwest of France, *J. Geophys. Res.*, this issue.

Kaimal, J.C., and J.J. Finnigan, Atmospheric boundary layer flows, Their structure and measurement, 289 pp., Oxford University Press, New York, 1993.

Lagouarde, J.-P., Y. Brunet, and R.G.B. Andre, A simple PBL approach for estimating actual evapotranspiration from TIR data over a pine forest canopy, paper presented at the Workshop on Thermal Remote Sensing of the Energy and Water Balance Over Vegetation in Conjunction With Other Sensors, 5 pp., Penn State Univ./CEMAGREF/CRPE, La Londe Les Maures, France, 20-23 September, 1993.

Lopez A., J. Fontan, M.O. Barthomeuf, and A. Minga, Présentation de l'expérience Atila: Action des terpènes et de l'isoprène dans l'atmosphère (forêt des Landes), *Atmos. Environ., 22*, 1881-1894, 1988.

McMillen, R.T., An eddy correlation technique with extended applicability to non-simple terrain, *Boundary Layer Meteorol., 43*, 231-245, 1988.

Owen, P.R., and W.R. Thompson, Heat transfer across rough surfaces, *J. Fluid Mech., 15*, 321-344, 1963.

Panofsky, H.A., H. Tennekes, D.H. Lenshow, and J.C. Wyngaard, The characteristics of turbulent velocity components in the surface layer under convective conditions, *Boundary Layer Meteorol.*, 11, 355-361, 1977.

Serça, D., R. Delmas, C. Jambert, and L. Labroue, Emissions of nitrogen oxides from equatorial rainforest in Central Africa, Origin and regulation of NO emissions from soils, *Tellus*, in press, 1994.

Sievering, H., Small particle dry deposition under high wind speed conditions: Eddy flux measurements at the Boulder Atmospheric Observatory, *Atmos. Environ., 20*, 2179-2185, 1987.

Simon, V., B. Clément, and M.-L. Riba, and L. Torres, The Landes experiment: Monoterpenes emitted from the maritime pine, *J. Geophys. Res.*, this issue.

Slinn, W.G.N., Prediction of particle deposition to vegetative canopies, *Atmos. Environ., 16*, 301-306, 1982.

Song-Miao, F., S.C. Wofsy, P.S. Bakwin, and D.J. Jacob, Atmosphere-biosphere exchange of CO_2 and O_3 in the central Amazon forest. *J. Geophys. Res., 95*, 16,851-16,864, 1990.

Thom, A.S., Momentum absorption by vegetation, *Q. J. R. Meteorol. Soc., 97*, 414-428, 1971.

Wesely, M.L., Parametrization of surface resistance to gaseous dry deposition in regional-scale numerical models, *Atmos. Environ., 23*, 1292-1304, 1989.

Wesely, M.L., D.R. Cook, and R.L. Hart, Fluxes of gases and particles above a deciduous forest in wintertime, *Boundary Layer Meteorol., 27*, 237-255, 1983.

Wesely, M.N., D.R. Cook, and R.L. Hart, Measurements and parameterization of particulate sulfur dry deposition over grass, *J. Geophys. Res., 90*, 2131-2143, 1985.

Y. Brunet, Laboratoire de Bioclimatologie, INRA, BP 81, 33883 Villenave d'Ornon Cédex, France. (e-mail: brunet@bordeaux.inra.fr)

A. Druilhet, J. Fontan, A. Labatut, E. Lamaud, and A. Lopez, Laboratoire d'Aérologie, Unité Associée CNRS 353, Université Paul Sabatier, 118, route de Narbonne, 31062 Toulouse Cédex, France.

(Received August 18, 1993; revised February 12, 1994; accepted March 10, 1994.)